Kinome Profiling of Gastrointestinal Stromal Tumors Using Multiplexed Inhibitor Beads and Mass Spectrometry Identifies Wee1 as Candidate Therapeutic Target

Shuai Ye[1], Dinara Sharipova[1], Marya Kozinova[1,2], Lilli Klug[3], Jimson D'Souza[1], Martin G. Belinsky[1], Katherine J. Johnson[4], Margret B. Einarson[1], Kathy Cai[4], Karthik Devarajan[5], Yan Zhou[5], Samuel Litwin[5], Michael C. Heinrich[3], Ronald DeMatteo[6], Margaret von Mehren[1], James Duncan[4] and Lori Rink[1*]

[1]Molecular Therapeutics Program, Fox Chase Cancer Center, Philadelphia, Pennsylvania, USA

[2]Pirogov Russian National Research Medical University, Moscow, Russia

[3]Portland VA Health Care System and OHSU Knight Cancer Institute, Portland, OR

[4]Cancer Biology Program, Fox Chase Cancer Center, Pennsylvania, USA

[5]Department of Biostatistics and Bioinformatics, Fox Chase Cancer Center, Philadelphia, Pennsylvania, USA

[6]Department of Surgery, Perelman School of Medicine, University of Pennsylvania, Philadelphia, Pennsylvania, USA

*Correspondence to: Lori Rink, Ph.D., Molecular Therapeutics Program, Fox Chase Cancer Center, 333 Cottman Avenue, Philadelphia, PA 19111-2497, Phone: (215) 214-1608, FAX: (215) 728-2741

E-mail: Lori.Rink@fccc.edu

Running title: Kinome Profiling of GIST reveals new therapeutic targets

Abstract

Gastrointestinal stromal tumor (GIST) management has been revolutionized by the identification of activating mutations in *KIT* and *PDGFRA* and clinical application of receptor tyrosine kinase (RTK) inhibitors in advanced disease. Stratification of GIST into molecularly defined subsets provides insight into clinical behavior and response to approved targeted therapies. Although these RTK inhibitors are effective in most GIST, resistance remains a significant clinical obstacle. Development of effective strategies for refractory GIST requires identification of novel targets to provide additional therapeutic options. Global kinome profiling has potential to identify critical signaling networks and reveal protein kinases that are essential in GIST. Using Multiplexed Inhibitor Beads and Mass Spectrometry paired with a super-SILAC kinome standard, we explored the majority of the kinome in GIST specimens from the three most common molecular subtypes to identify novel kinase targets. Kinome profiling revealed distinct signatures in GIST subtypes. *PDGFRA*-mutant GIST had elevated tumor associated macrophage (TAM) kinases and immunohistochemical analysis confirmed increased TAMs present in these tumors. Kinome profiling with loss-of-function assays revealed a significant role for G2-M tyrosine kinase, Wee1, in GIST survival. *In vitro* and *in vivo* studies revealed significant efficacy of MK-1775 (Wee1 inhibitor) in combination with avapritinib in *KIT* and *PDGFRA*-mutant GIST cell lines, and notable efficacy of MK-1775 as a monotherapy in the *PDGFRA*-mutant line. These studies provide strong preclinical justification for the use of MK-1775 in GIST.

Introduction

Gastrointestinal Stromal Tumors (GIST) are the most common mesenchymal tumors of the gastrointestinal tract, with 5000-6000 new cases diagnosed in the US per year (1). These tumors are characterized by the near-universal expression of the receptor tyrosine kinase (RTK) KIT, and the majority of GIST harbor constitutively active mutant isoforms of either KIT (70-80%) or the related RTK, PDGFRA (5-7%) (2). The ~10-15% of GIST that lack mutations in these genes often exhibit genetic or epigenetic deficiencies in the succinate dehydrogenase (SDH) complex of the respiratory chain (3, 4), and are referred to as SDH-deficient (SDH-d). Therapeutic targeting of GIST with front-line RTK inhibitor imatinib mesylate (IM) along with two other FDA approved agents (sunitinib and regorafenib) has transformed therapy for advanced, unresectable GIST. However, this "one size fits all" approach to GIST treatment fails to address the molecular and clinical heterogeneity of these tumors. Tumor genotype has been shown to be an independent prognostic factor as well as a predictor of IM response in GIST (5). The majority of GIST harbor mutations in *KIT* that affect the juxtamembrane domain encoded by exon 11. While tumors with mutations in this region generally respond well initially to IM therapy, they may exhibit negative prognostic features and aggressive biology (6). In contrast, *PDGFRA*-mutant and SDH-d GIST may exhibit a more indolent clinical course than *KIT*-mutant tumors (7), however these GIST subtypes often demonstrate little or no response to IM (8, 9) or to other approved therapies. The most common *PDGFRA* mutation found in GIST, the D842V substitution, is particularly insensitive to IM. Avapritinib (BLU-285, Blueprint Medicines), a highly selective inhibitor of *KIT* exon 17 and *PDGFRA* exon 18 activation loop mutants, has demonstrated efficacy *in vitro* (10) and *in vivo* (11). Phase I testing (NAVIGATOR study, NCT02508532) has demonstrated notable efficacy for exon 18 *PDGFRA*-mutant GIST as well as fourth-line *KIT* mutant GIST patients (12),

4

leading to FDA approval for the use of avapritinib in unresectable or metastatic *PDGFRA* exon 18-mutant GIST in January 2020.

Although these RTK inhibitors are effective in the majority of GIST, primary and acquired resistance to these agents remains a significant clinical obstacle. For clinical management of refractory GIST to improve, new therapeutic targets must be identified. Finding a better way forward will require a more complete understanding of how the particular molecular aberrations in these GIST subsets affect tumor signaling pathways and ultimately impact clinical behavior and therapeutic response. Differences in global gene expression and genomic profiles have been reported for GIST subtypes (3, 13, 14), however kinome profiling of GIST has not been performed to date. Global kinome profiling has the potential to identify essential signaling networks and reveal protein kinases that are critical in GIST. Protein kinases are highly druggable, with more than 45 FDA approved kinase inhibitors (15), the majority of which are used in the clinic to treat malignancies. Notably, a large fraction of the kinome remains untargeted and understudied in cancer (16). Several chemical proteomics approaches have been developed that measure levels of a significant proportion of the kinome in cells and tissues, including Kinobeads, Kinativ and Multiplexed Inhibitor Beads and Mass Spectrometry (MIB-MS) (17-19). MIBs consists of a layered mixture of immobilized ATP-competitive pan-kinase inhibitors that enriches endogenous protein kinases from cell lysates based on the affinity of individual kinases for the different immobilized inhibitors, their kinase abundance, and/or the activation state of the kinase (18).

In this work, using Multiplexed Inhibitor Beads and Mass Spectrometry (MIB-MS) paired with a super-SILAC (s-SILAC) kinome standard (20, 21), we explored the majority of the kinome in

5

treatment naïve primary GIST specimens from three GIST subtypes (*KIT*-mutant, *PDGFRA*-mutant and SDH-d GIST) in order to identify potential novel kinase targets. Using this proteomics approach, we demonstrated that the three GIST subtypes have distinct kinome profiles, and identified kinases that are universally activated in all GIST, as well as kinases that are unique to each subtype. Interestingly, kinome profiling of the *PDGFRA*-mutated subtype of GIST revealed enhanced signaling pathways involved in innate immune response activation and inflammation. To correlate these findings, we showed significantly increased levels of tumor associated macrophages (TAM) in the *PDGFRA*-mutated subtype compared to other GIST subtypes. Finally, kinome profiling in combination with loss-of-function validation assays revealed a significant role for the G2-M tyrosine kinase, Wee1, in GIST survival. We also report significant efficacy of MK-1775 (Wee1 inhibitor) as a single agent, and in combination with avapritinib in a novel GIST cell line driven by an activating *PDGFRA* D842V mutation as well as in an isogenic cell line driven by a *KIT* mutation. The combination was also effective in controlling the growth of these PDGFRA-driven GIST cells in 3-dimensional spheroid culture. Furthermore, dual inhibition of Wee1 and KIT/PDGFRA in GIST xenografts provided impressive, extended disease stabilization and improved survival.

Material and Methods

Kinome Profiling Experimental Design, Data Analysis and Statistical Rationale- For proteomic measurement of kinase abundance in primary GIST, we applied MIB-MS kinome profiling coupled with a super-SILAC (s-SILAC) approach, as previously described (20). Five milligrams of each primary GIST were mixed 1:1 with the s-SILAC reference sample, endogenous kinases purified by MIB-resins, kinases eluted, digested, and peptides analyzed by LC/MS-MS. Kinase protein levels in tissues were quantitated by comparing s-SILAC-labeled peptides from s-

6

SILAC reference with non-labeled peptides from tissues using MaxQuant. For MIB-MS data analysis, MaxQuant normalized ratios were imported into Perseus software (1.6.2.3) for quantification. MIB-MS profiles were processed in Perseus software in the following manner: normalized MIB-MS s-SILAC ratios were transformed $1/(x)$ to generate light / heavy ratios, followed by $\log2/(1/x)$ transformation. Rows were filtered for minimum valid kinases measured in at least 50% of MIB-MS runs. Imputation of missing values was perfomed as previously described (22), where in the s-SILAC data, a width of 0.3 and the downshift of 0.5, was employed. Principal component analysis (PC1 vs PC2, PC2 vs PC3 and PC1 vs PC3) was then performed to visualize kinome profiles amongst samples using the following parameters; Number of components: 5, Cutoff method: Benjamini-Hochberg FDR 0.05 and Relative enrichment: none. Hierarchical clustering (Euclidean) of s-SILAC ratios was performed with parameters Linkage: average and Constrait: none. Difference in kinase abundance among GIST (n=33), *KIT*-mutant (n=15), *PDGFRA*-mutant (n=10), SDH-d (n= 8) and normal gastric tissue (n=9) was determined using two-sample Student's t-test with the following parameters (S0: 0.1 and Side: Both, Benjamini-Hochberg FDR 0.05) using Perseus software.

Nano-LC-MS/MS- Proteolytic peptides were resuspended in 0.1% formic acid and separated with Thermo Scientific RSLC Ultimate 3000 on Thermo Scientific Easy-Spray C18 PepMap 75μm x 50cm C-18 2 μm column with a 240 min gradient of 4-25% acetonitrile with 0.1% formic acid at 300 nL/min at 50°C. Eluted peptides were analyzed by a Thermo Scientific Q Exactive plus mass spectrometer utilizing a top 15 methodology in which the 15 most intense peptide precursor ions were subjected to fragmentation. The AGC for MS1 was set to 3×10^6 with a max injection

time of 120 ms, the AGC for MS2 ions was set to 1×10^5 with a max injection time of 150 ms, and the dynamic exclusion was set to 90s.

Data Processing - Raw data analysis of super-SILAC experiments was performed using Maxquant software 1.5.3.30 and searched using andromeda 1.5.6.0 against the swiss-prot human protein database (downloaded on September 25, 2015). The search was set up for full tryptic peptides with a maximum of two missed cleavage sites. All settings were default and searched using acetylation of protein N-terminus and oxidized methionine as variable modifications. Carbamidomethylation of cysteine was set as fixed modification. The precursor mass tolerance threshold was set at 10 ppm and maximum fragment mass error was 0.02 Da. SILAC quantification was performed using MaxQuant by choosing multiplicity as 2 in group-specific parameters and Arg10 and Lys8 as heavy labels. The match between runs was employed and the significance threshold of the ion score was calculated based on a false discovery rate of < 1%.

Data Availability- All mass spectrometry proteomics data have been deposited to ProteomeXchange Consortium via PRIDE partner repository with the dataset identifier PXD019210.

Immunohistochemical analysis- Tumor associated macrophages were assessed using an antibody recognizing CD68 (DAKO, Santa Clara, CA). Immunohistochemical staining was performed by the Fox Chase Cancer Center (FCCC) Clinical Pathology Laboratory on 5-μm slides as described previously (23). All IHC evaluation was performed in a blinded manner by one author (K.C). Immunohistochemical staining of CD68 was semi-quantitatively categorized as a score of 0, 1+

(mild）2+ (moderate) or 3+ (severe) for no CD68$^+$ cells, ≤10 CD68$^+$ cells, 11–20 CD68$^+$ cells or ≥21 CD68$^+$ cells in the observing field at ×200 magnification within the tumor.

Cell lines, compounds, and antibodies

The GIST-T1 tumor cell line possessing a heterozygous mutation in *KIT* exon 11 was kindly provided by Takahiro Taguchi (Kochi University, Kochi, Japan) (24). GIST-T1+Cas9 and GIST-T1+D842V KIT^{KO} are sublines of GIST-T1. GIST-T1+Cas9 was generated transduction of Cas9 using the LentiV-Cas9-puro vector system generously provided by Christopher Vakoc (Cold Spring Harbor Laboratory). The GIST-T1+D842V KIT^{KO} subline was created by transducing cells with D842V-mutant PDGFRA. Endogenous KIT expression was knocked-out using CRISPR/Cas9. Knockout was verified at protein and DNA levels. All GIST-T1 cell lines were grown in Iscove's Modified Dulbecco's Media (IMDM) with 10% FBS and were routinely monitored by Sanger sequencing to confirm their *KIT* /*PDGFRA* mutation status and cell identity. Cell lines were regularly tested for mycoplasma contamination by PCR and by MycoAlert Mycoplasma Detection Kit (Lonza). Avapritinib and MK-1775 were obtained from Selleckchem (Houston, TX). For *in vitro* experiments, avapritinib and MK-1775 were dissolved in DMSO. For *in vivo* experiments, avapritinib and MK-1775 were dissolved in 2% DMSO + 40% PEG400 + 2% Tween80 + ddH$_2$O. All antibodies used were purchased from Cell Signaling Technology, except β-actin and γ-H2AX (Millipore Sigma, St. Louis, MO).

siRNA transfection

The custom siRNA library was synthesized with four independent siRNAs pooled for each target (siGenome SMARTpool, Dharmacon, Lafayette, CO). Transfection conditions were determined for GIST-T1+Cas9 and GIST-T1+D842V KIT^{KO} cells using siRNA SMARTpools against KIT,

9

PDGFRA and GL-2 (Dharmacon) controls to achieve Z′ factor of 0.5 or greater. Reverse transfection mixtures were assembled in 96 well format with a final siRNA concentration of 50nM. After seventy-two hours, plates were assayed for cell viability using the CellTiter Blue (CTB) Viability Assay (Promega, Madison, WI). Assay readout was performed on a Perkin Elmer Envision multilabel plate reader after three hours of incubation with the CTB reagent.

Cell proliferation/viability assay

Tumor cells were plated in 96-well plates at optimal 0.6×10^4 densities and incubated overnight. Wells were treated in sextuplicate with varying doses of MK-1775 and/or avapritinib. Cell proliferation and viability were measured at 72 hours after treatment using CTB Assay as described above, at 4 hours after addition of CTB reagent. Assays were performed as three independent biological replicates, with minimum of three technical replicates in each treatment arm. An increasing dose series was used for each drug to estimate LD50. A function of form A + (1-A) * exp(-B*dose) or A + (1-A)/[1 + (dose/B)^p] was fitted to data by least squares. These functions were used to interpolate surviving fractions between those in the dose series and set to ½ to estimate corresponding LD50s, (LD50-1 and LD50-2). Increasing series of combination doses in the same ratio were used as their LD50s to estimate the LD50 of that combination (dose1 and dose2), using an interpolating function. If the combination index, CI = dose1/LD50-1 + dose2/LD50-2 < 1 then the point (dose1, dose2) may be synergistic, otherwise, it was considered either additive or antagonistic. If not considered additive or antagonistic, a bootstrap resampling method was used to test the null hypothesis of no synergism (25).

Spheroid drug sensitivity

Spheroids were formed in 96 Well U-Bottom Clear Cell Repellent Surface Microplates (Greiner Bio-One). GIST-T1+Cas9 and GIST-T1+D842V KIT^{KO} cells were suspended in complete IMDM (4,500 cells/well) for 24 hours for spheroid formation. Spheroids were treated with appropriate drug(s) in 50-µL complete IMDM. Spheroids were imaged at 4× magnification by EVOS FL Digital Inverted Microscope (AMG) after 120 hours of drug treatment. Spheroid surface area and spheroid viability was measured as described previously (26). Three independent biological replicate experiments were performed with a minimum of three technical replicates in each treatment arm. Statistical analyses were conducted as described previously (26).

BrdU incorporation assay

DNA synthesis proliferation rate was measured using BrdU Flow kit (BD Biosciences, San Jose, CA) according to manufacturer's protocol. Treated GIST-T1+Cas9 and GIST-T1-D842V+KIT^{KO} cells were labelled with bromodeoxyuridine (BrdU) for 3.5 h. Anti-FITC-BrdU antibody was used in GIST-T1+Cas9 cells and anti-APC-BrdU was used in GIST-T1-D842V+KIT^{KO} cells. Total DNA was stained with 7-amino-actinomycin D (7-AAD). Double labeled samples were analyzed using two-color flow cytometric analysis conducted on LSR ll BD flow cytometer. Data was analyzed and displayed using FlowJo software.

Preparation of whole cell extract from cells and immunoblot assays

The whole cell extracts were prepared and evaluated by immunoblot assay as described previously (27).

GIST xenografts and drug administration

11

All studies involving animals followed procedures approved by the FCCC Institutional Animal Care and Use Committee. GIST-T1+Cas9 and GIST-T1+D842V KIT^{KO} cells were washed and resuspended in PBS at a density of 1×10^6 cells/100 µL. One hundred microliters of cells in PBS were mixed thoroughly with 100 µL of Matrigel Matrix (BD Biosciences) and the suspension was injected subcutaneously into the right flanks of SCID mice (CB.17/SCID, Taconic Biosciences). Tumor volume was calculated as described previously (26). When tumors reached approximately 300 mm^3, mice were randomized into five treatment arms: arm 1, vehicle; 2, MK-1775 at 60 mg/kg, twice a day (oral); arm 3 avapritinib 10mg/kg, once a day (oral) and arm 4, combination of MK-1775 and avapritinib at monotherapy doses. Treatment was continued until the tumors exceeded >10% of their body weight or the animals demonstrated distress or weight loss >10%.

Tumor growth modeling

Tumor volume was measured for every mouse in all four treatment arms (vehicle, MK-1775, avapritinib and combination) at a total of 15 distinct time points in GIST-T1+Cas9 xenografts, from baseline (Day 0) until study conclusion (47 Days) and 25 distinct time points in GIST-T1+D842V KIT^{KO} xenografts, from baseline (Day 0) until study conclusion (Day 89). A longitudinal model based on the generalized estimating equations approach (Gaussian model with identity link and an autoregressive correlation structure) was used to model the effect of treatment and time on (the logarithm of) tumor volume. A linear time-effect was included in the model for the logarithm of tumor volume and interacted with treatment. Disease specific survival and tumor volume were compared between treatment groups using the log rank and Mann–Whitney tests, respectively. All tests were two-sided and used a type I error of 5%. The package geepack and survival in the R statistical language and environment was used in these computations.

12

Results

Kinome profiling of primary GIST using MIB-MS

In order to explore the kinome landscapes among the three molecular subtypes of GIST, we profiled 33 IM-naïve primary gastric GIST specimens which include the following GIST subtypes: 1) *KIT* exon 11 mutants (N=15), 2) *PDGFRA* mutants (N=10) and 3) *KIT/PDGFRA*-wild-type (WT) GIST (N=8) using MIB-MS (**Table 1)**. The *KIT/PDGFRA*-WT GISTs include 7 SDH-d and one GIST that lacked *SDH* mutations and was shown to be SDH intact as indicated by SDHB immunohistochemistry (28). In addition, we kinome profiled 9 normal gastric tissues from donors that had no history of kinase inhibitor therapy. Briefly, a super-SILAC "heavy" kinome reference sample (21, 29) was spiked into "light" tissue sample lysates, kinases enriched using MIB-columns, eluted, trypsin digested, and kinase peptides analyzed by LC-MS/MS. Kinase abundance in tissues was quantitated by comparing kinase s-SILAC-labeled peptides with non-labeled peptides from tissues using MaxQuant software (**Figure 1A)**. In total, we measured MIB-binding values for 326 kinases across these GIST samples, with 205 kinases quantitated in >50% of tissues profiled and 102 kinases measured in every MIB-MS run. The average number of kinases measured for each sample was 205, with normal gastric tissues exhibiting the fewest kinases quantitated per run (**Figures 1B,_C**, and **Data file S1**). Principal component analysis (PCA) and hierarchical clustering of MIB-MS profiles revealed that the kinome of GIST primary tumors is overall distinct from normal gastric tissues (**Figures 1D-E**). Furthermore, PCA of the kinome profiles revealed *KIT*- and *PDGFRA*-mutant GIST tumors grouped distinctly from KIT/PDGFRA WT GIST (**Figure 1D**). One exception to this was a *KIT/PDGFRA* wild-type (WT16) sample that clustered closer to the *KIT*-mutant GIST samples. Interestingly, this sample was distinct from the

13

other KIT/PDGFRA WT GIST samples in that it possessed an intact SDH complex, and most likely has an unknown driver mutation. Notably, GIST tumors harboring the *PDGFRA* mutation grouped together among other tumors, with 8 of 10 tumors forming a distinct cluster, suggesting these tumors expressed a distinct kinome pattern (**Figures 1D-E**).

Mapping the distinct kinome signatures among GIST subtypes

Volcano plots depict kinases uniquely elevated or reduced among the GIST subytpes (**Figures 2A-C**). IGF1R was the top ranking kinase activated in *KIT/PDGFRA*-wild-type (11.3 fold) versus *KIT*- and *PDGFRA*-mutant subtypes, as previously described (30, 31) (**Figure 2A**).   Notably, *PDGFRA*- and *KIT*-mutant GIST samples exhibited elevated MIB-binding of several established driver kinases relative to GIST-WT tumors, including SRC-family kinases SRC, LYN, FRK, and FES (32, 33), as well as CDK4 and MAPK3 (ERK1) consistent with increased growth and metastatic properties of GIST-mutant tumors (34, 35).

MERTK and AXL, tumor associated marophage (TAM) kinases, were identified as significantly elevated in the *PDGFRA*-mutant subtype compared to *KIT*-mutant and *KIT/PDGFRA*-WT subtypes (**Figures 2C-E**). Using immunohistochemical analysis of CD68, a protein highly expressed in macrophages, we interrogated the presence of TAMs in formalin fixed parrafin-embedded (FFPE) specimens from untreated *KIT*-mutant (N=8) and *PDGFRA*-mutant (N=8) primary GIST. The CD68 score was significantly higher in the *PDGFRA*-mutant group as compared to *KIT*-mutant tumors (**Figures F-G**), comfirming the elevated presence of TAMs in this subtype. In addition, Lymphocyte-specific Kinase (LCK) was also significantly activated in *PDGFRA*-mutant group compared to other GIST subtypes (**Figures 2C-E**). These findings are in

14

accordance with a recent report from Vitiello et al. (36) demonstrating increased immune cells present in the *PDGFRA*-mutant GIST compared to the *KIT*-mutant group. To characterize expression of MERTK, AXL and LCK, we queried an independently performed RNA-seq study of 23 *KIT*- and 16 *PDGFRA*-mutant primary GIST (36). Statistically significant elevated expression of all three kinases was observed in the *PDGFRA*-mutant group compared to *KIT*-mutant counterparts (**Figure 2H).**

Targeting the GIST tumor kinome signature identifies WEE1 as candidate target

As expected, a volcano plot showed significant differences between normal gastric tissue and all GIST, including significant elevation of KIT, PRKCQ and FGFR1, all of which have been previously shown to be up-regulated in GIST, and hence served to improve our confidence in the validity of these data (37, 38) (**Figure 3A)**. To explore the functional relevance of the identified kinases from our kinome profiling studies, we designed a kinase-centric siRNA library to identify kinases that are critical for *KIT*- and *PDGFRA*-mutant GIST cell survival. This siRNA library contained pooled siRNAs targeting each of the 94 kinases identified in the kinome profiling experiment described above. Synthetic lethal screens were performed using an isogenic pair of cell lines: GIST-T1+Cas9 (KIT driven) and GIST-T1+D842V KIT^{KO} (PDGFRA D842V driven). Positive controls for the screen included siKIT (GIST-T1+Cas9) and siPDGFRA (GIST-T1+D842V KIT^{KO}), while siGL2 served as negative control for both lines (**Figure S1**). Hits from the screen identified 12 unique kinases in the PDGFRA-driven group, 8 kinases in the KIT-driven group, and 66 kinases that appear to be critical for both *KIT*- and *PDGFRA*-mutant GIST survival (**Figure 3B)**. Using hit criteria of >20% cytotoxicity score (with an FDR<5) we selected the top 19 kinases to move forward for further evaluation. Quantititative PCR analysis confirmed

15

knockdown of the target in 18/19 kinases (**Figures S2, S3).** Notably, knockdown of Wee1, a serine/threonine kinase central to the G2/M checkpoint, was found to induce significant cytotoxicity in both cell lines (52.3% in GIST-T1+Cas9; 58.6% in GIST-T1+D842V KIT^{KO}) , with viabilty scores approaching levels similar to KIT and PDGFRA positive controls (**Figure 3B)**. Greater than seventy percent Wee1 knockdown was achieved in both cell lines (**Figure 3C**).

MK-1775 and avapritinib have enhanced combination effects on *in vitro* GIST cell growth

Although avapritinib has demonstrated dramatic responses in *PDGFRA*-mutant GIST harboring the D842V mutation and in IM-refractory *KIT*-mutant GIST in clinical trials, acquired resistance to this monotherapy is likely. A large body of evidence suggests that targeting multiple pathways may be a more successful route. Given the promising kinome profiling data which demonstrated increased Wee1 activation in GIST (**Figure 3D**) and the significant effect on cell viability associated with Wee1 knockdown (**Figure 3B**), we next tested the effects of combined inhibition of Wee1, using MK-1775, a commercially available selective inhibitor of Wee1, with KIT/PDGFRA inhibition using avapritinib. We evaluated the effects of MK-1775 and avapritinib using the GIST-T1+Cas9 (KIT driven) and GIST-T1+D842V KIT^{KO} (PDGFRA driven) cell lines, as single agents and in combination at increasing molar ratios. **Figures 4A and B** show single agent dose response curves for GIST-T1+Cas9 and GIST-T1+D842V KIT^{KO}, respectively. We first estimated the LD50 for each agent in the two cell lines (**Figures 4A** and **B, left panels**). We then treated each line with increasing doses of the two drugs in a fixed ratio as their LD50s (**Figures 4A** and **B**, **third panel**). To quantify synergy of the two drugs, combination index (CI) values were calculated (**Figures 4A** and **5B, last panel:** CI values <1 are considered synergistic). The CI$_{LD50}$ values for GIST-T1+Cas9 (KIT driven) and GIST-T1+D842V KIT^{KO} were 1.06 and

0.589, respectively, indicating possible synergy only in the PDGFRA-driven cell line, which was then established to be significant via a bootstrap statistic (see Methods) (25). Although synergy was not observed in the GIST-T1+Cas9 cell line, a clear additive effect of the two drugs was detected. Interestingly, querying the independent RNA-seq study as described above revealed *PDGFRA*-mutant GIST displayed elevated Wee1 expression compared to *KIT*-mutant GIST, however statstical significance was not reached (**Figure 2G**) .

To evaluate the effects of the drugs as single agents or in combination on 3D GIST cell growth, spheroid assays were performed which more accurately mimic tumor physiology than cells grown in monolayer. GIST-T1+Cas9 and GIST-T1+D842V KIT^{KO} cells form dense, uniformly spherical cultures with true cell-to-cell contacts that are maintained upon physical manipulations, indicative of true speroids (**Figure 4E**). Treatment of both GIST-T1+Cas9 and GIST-T1+D842V KIT^{KO} spheroids with either of the single agents, MK-1775 (700 nM) or avapritinib (40 nM), resulted in decreased spheroid viability (**Figure 4C**) and volume (**Figures 4D,E**) relative to vehicle-treated spheroids (**Figure 4E**). However, treatment of these spheroids with the combination resulted in a significantly greater reduction in both viability and volume (**Figures 4C, D, E**). Interestingly, both MK-1775 as a single agent and in combination with avapritinib had greater efficacy in GIST-T1+D842V KIT^{KO} compared to GIST-T1+Cas9 spheroids.

Combination treatment increases DNA damage and apoptosis

The effect of pharmacological inhibition of KIT/PDGFRA and Wee1 on cell cycle dynamics in GIST cells was measured with a BrdU assay. GIST-T1+Cas9 and GIST-T1+D842V KIT^{KO} cells treated with vehicle (control), MK-1775, avapritinib or the combination were analyzed by flow

17

cytometry after BrdU incorporation and subsequent antibody binding in combination with direct

7-AAD staining **(Figures 5A, B)**. MK-1775 treatment induced G2-phase cell cycle arrest in GIST-

T1+Cas9 cells, whereas cells treated with avapritinib exhibited significant G0/G1-phase arrest

compared to control cells. GIST-T1+Cas9 cells treated with the combination exhibited increased

subG1 population indicating increased apoptosis compared to either monotherapy treatment group

(Figure 5A). Conversely, MK-1775 induced G0/G1-phase arrest in GIST-T1+D842V KIT^{KO} cells

whereas avapritinib induced G2 arrest compared to control cells. Combination treatment

significantly increased the subG1 population compared to either monotherapy group **(Figure B)**.

The subG1 population was two-fold higher in combination-treated GIST-T1+D842V KIT^{KO} cells

compared to GIST-T1+Cas9 cells. In order to interrogate the mechanism of action of these

inhibitors, we performed immunoblotting on GIST cell lines treated with MK-1775, avapritinib,

or the combination **(Figure 5C)**. Following avapritinib treatment, inhibition of KIT and PDGFRA

was observed in GIST-T1+Cas9 and GIST-T1+D842V KIT^{KO}, respectively. Wee1 typically

inhibits CDC2 (cell division cycle protein 2; also known as cyclin dependent kinase 1 (CDK1))

activity by phosphorylating it on two different sites, Tyr15 and Thr14, thereby decreasing its

kinase activity and preventing entry into mitosis. Treatment with MK-1775 led to significant

inhibition of Tyr15 on CDC2 **(Figure 5C)**. Interestingly, both GIST-T1+Cas9 and GIST-

T1+D842V KIT^{KO} cells treated with MK-1775 alone or in combination with avapritinib

demonstrated increased γ-H2AX and cleaved-PARP, suggesting increased DNA double-strand

breaks and apoptosis. We hypothesize that this increased DNA damage may be a result of loss of

cell cycle checkpoints and decreased time for DNA repair mechanisms ultimately causing

increased cell death. Interestingly, the KIT-independent cell line, GIST-T1+D842V KIT^{KO}, has

significantly more cyclin D1 than the KIT-dependent line, GIST-T1+Cas9, in accordance with a

18

recent report (39), providing a potential explanation for the differential effects of MK-1775 and avapritinib in these two cell lines.

Combination treatment reduces tumor growth and improves survival *in vivo*

On the basis of these strong *in vitro* data, we hypothesized that there would be benefit in simultaneously inhibiting KIT/PDGFRA and Wee1 leading to loss of cell cycle checkpoint arrest, increased DNA damage and ultimately increased cell death. To test this hypothesis, we performed a GIST xenograft study under a FCCC Institutional Animal Care protocol using the GIST-T1+Cas9 and GIST-T1+D842V KIT^{KO} cell lines. Xenografts were established subcutaneously in a total of 32 C.B17 SCID mice per cell line and randomized into four treatment arms: arm 1: vehicle, arm 2: MK-1775, arm 3: avapritinib and, arm 4: avapritinib/MK-1775 combination. GIST-T1+Cas9 xenografts showed significant disease stabilization in both the avapritinib monotherapy ($p = 0.05$) and avapritinib/MK-1775 combination ($p = 0.002$) arms compared to all other groups **(Figure 6A).** Significant disease stabilization was observed in GIST-T1+D842V KIT^{KO} xenografts in both avapritinib ($p = 0.002$) and MK-1775 ($p = 0.02$) monotherapy arms **(Figure 6B).** Combination treated GIST-T1+D842V KIT^{KO} tumors showed disease stabilization and tumor regression ($p = < 0.0002$) at day 15 **(Figure 6B).** Importantly, GIST-T1+Cas9 tumor response led to significant improvement in disease-specific survival in the avapritinib/MK-1775 combination treated group ($p = <0.0001$) compared to vehicle group **(Figure 6C).** Kaplan-Meier curves for disease-specific survival of GIST-T1+D842V KIT^{KO} tumors demonstrate that avapritinib/MK-1775 combination-treated mice survived significantly longer than all other mice, including avapritinib alone **(Figure 6D).** Impressively, at the end of the study (89 days) 75% of the combination treated mice were still alive, one without a measureable tumor, when no other vehicle

19

and montherapy treated mice were alive. After treatment discontinuation, we observed regrowth of these tumors after approximately four weeks in all but one mouse, whose tumor never regrew.

Discussion

Historically, treatment for advanced GIST involved the sequential application of IM, sunitinib, and regorafenib, regardless of genotype. This approach provided initial benefit to particular molecular subsets of GIST (e.g. *KIT* mutants) and little to no benefit to others (e.g. *PDGFRA* D842V mutants). An increased understanding of GIST biology has revealed clear heterogeneity among the molecular subtypes and a corresponding need for novel therapeutics to target subtype-specific GIST. Recently, this has been borne out with the success of avapritinib in the treatment of *PDGFRA* D842V-mutant GIST, prompting FDA approval of avapritinib as front-line therapy for this subtype in the unresectable or metastatic setting (12). While the application of inhibitors targeting the primary mutant isoforms of KIT and PDGFRA has revolutionized the treatment of GIST, acquired resistance remains a significant clinical challenge. Addressing this challenge may require the identification and targeting of additional protein kinases within cancer-promoting cell signaling pathways that are active within GIST sub-types.

In this study, we utilized a novel chemical proteomics approach, a SILAC-based MIB-MS platform, to profile the kinome of human gastric GIST specimens along with normal gastric tissue. This platform provides a quantitative assessment of kinase abundance for nearly 65% of the human kinome. The kinomes of GIST primary tumors exhibit both a higher level of quantifiable activated kinases, and a distinct profile, as compared to normal gastric tissues. This was not surprising since GIST are generally characterized by gain-of-function mutations that activate multiple signaling pathways. Kinome profiling also revealed significant differences between RTK-mutant

20

(*KIT/PDGFRA)* GIST tumors and SDH-d GIST that lack these mutations. This was expected given the distinct biology of KIT/PDGFRA-driven tumors and SDH-deficient GIST (23, 40). Surprisingly, we also found that *PDGFRA*-mutant GIST tumors expressed a distinct kinome pattern compared to *KIT*-mutant tumors. Interestingly, these differences are partly due to elevated immune cell-associated kinases including MERTK, AXL and LCK, and the correlating increased TAMs observed by IHC in treatment-naïve *PDGFRA*- mutant compared to *KIT*-mutant GIST. Two recent reports (36, 41) have used RNA-seq to obtain immune profiles in GIST. Vitiello *et al*. (36) profiled 75 GIST (N= 37 *KIT*- and 24 *PDGFRA*-mutant) and observed significantly more immune cells present in the *PDGFRA* cohort. While Pantaleo *et al*. (41) did not report genotype specific differences in immune infiltrates in their cohort, their sample size was significantly smaller (N= 21 *KIT*- and 10 *PDGFRA*-mutant), and some of these cases had IM treatment or were classified as unknown treatment status, which could potentially influence the number and activity of immune infiltrates. TAMs have been shown to play an important role in GIST microenvironment and to be altered by IM treatment (42, 43). Interestingly, Zhang *et al*. (44) reported that the combination of IM and an agonistic antibody, anti-CD40, which activates TAMs, increased antitumoral effects of IM in a preclinical *KIT*-mutant GIST model. Our data, together with these other published reports, indicate that *PDGFRA*-mutant GIST may benefit from manipulation of TAMs to augment the effects of avapritinib.

Our GIST kinome profiling identified several well-studied and established kinases, such as KIT, PRKCQ (37) and FGFR1 (38), as significantly activated kinases in all GIST compared to normal tissue. In addition, our profiling identified Wee1, gatekeeper of the G2/M cell cycle checkpoint and largely understudied kinase in GIST, to be highly abundant in tumors compared to normal

21

tissue. Wee1 has been reported to be highly expressed in numerous malignancies including breast, hepatocellular, lung, melanoma and others (45), and the Wee1 inhibitor MK-1775 (adavosertib, AZD1775) has been evaluated in numerous preclinical and clinical trials as single agent or in combination, often with DNA damaging agents (46-48). Our loss-of-function studies targeting Wee1 in an isogenic pair of cell lines driven by KIT (GIST-T1+Cas9) or PDGFRA (GIST-T1+D842V KIT^{KO}) revealed an essential role for Wee1 in GIST cell proliferation, suggesting Wee1 as a plausible drug target in GIST. We demonstrated enhanced drug combination effects between avapritinib and MK-1775 in both KIT and PDGFRA-driven cell lines using two-dimensional (2D) and three-dimensional (3D) *in vitro* viability studies. Whereas additive effects of the combination were observed in GIST-T1+Cas9 cells, strong synergy was observed in GIST-T1+D842V KIT^{KO} cells treated with the combination. BrdU assays indicated significant differences in the effects of both MK-1775 and avapritinib on cell cycle between the two cell lines, and significantly enhanced apoptosis in the PDGFRA-driven cell line compared to its KIT-driven counterpart. We believe that these differences are due in part to differential expression of cyclin D1, a regulator of the G1/S cell cycle checkpoint, which was recently identified as an oncogenic mediator in KIT-independent GIST (38). Increased expression of γH2AX suggests increased DNA damage, most likely due to loss of cell cycle checkpoint, is responsible for enhanced cell death in combination treated cells.

The results of these *in vitro* studies provided justification for investigating such an approach *in vivo* to determine whether this combination would improve efficacy of avapritinib and/or increase time to resistance in GIST xenografts. Similar to the *in vitro* studies, the avapritinib+MK-1775 combination was significantly better at repressing tumor growth compared to both single agents in

22

both xenograft models, however, tumor regression was only observed in the GIST-T1+D842V KIT^{KO} line. Interestingly, MK-1775 alone had a significant effect on tumor volume compared to vehicle in only the PDGFRA-driven xenografts, indicating inherent cell cycle differences in KIT- versus PDGFRA-driven GIST. These differences were most noticeable when examining disease-specific survival. Impressively, at the end of the study (89 days) in the combination treated arm, 75% of the mice were alive, whereas no other mice, including in avapritinib monotherapy group, survived. Together, these xenograft studies provide strong evidence for the initiation of future clinical studies evaluating the use of avapritinib in combination with Wee1 inhibitors in patients with *PDGFRA*-mutant GIST and IM-refractory *KIT*-mutant GIST.

During the preparation of this manuscript, Liu *et al*. (49) published a report examining Wee1 in GIST. They reported elevated expression of Wee1 in GIST compared to normal gastric tissues and a significant anti-proliferative effect of Wee1 knockdown and MK-1775 treatment with DNA damage induction and increased apoptosis. These findings concur with our findings. However, their studies involved *KIT*-mutant GIST only. Our work indicates that in addition to *KIT*-mutant GIST, Wee1 may be a more promising target in *PDGFRA*-mutant GIST. We also hypothesize that Wee1 could be a novel target in SDH-d GIST based on our kinome profiling data and its independence of KIT. Furthermore, we expanded our analysis to include not only *PDGFRA*-mutant GIST but also to *in vivo* studies of MK-1775, while Liu *et al*. limited studies to *in vitro* evaluations of MK-1775 in *KIT*-mutant GIST. Therefore, our work underscores and expands the evidence for Wee1 serving an important role in GIST biology. And importantly, our data provides strong rationale for Wee1 as a novel therapeutic target in all subtypes of GIST.

23

Table 1: Genotype information for GIST patient samples		
Sample number[a]	Group	Mutation(s)[b]
KIT 08	KIT mutant	*KIT* exon 11: p.Val559Ala
KIT 09	KIT mutant	*KIT* exon 11: p.Val559Asp
KIT 11	KIT mutant	*KIT* exon 11: p.Val560Asp
KIT 13	KIT mutant	*KIT* exon 11: p.Val559Pro
KIT 20	KIT mutant	*KIT* exon 11: p.Val560Asp
KIT 21	KIT mutant	*KIT* exon 11: p.Val560Asp
KIT 22	KIT mutant	*KIT* exon 11: p.Trp557Arg
KIT 31	KIT mutant	*KIT* exon 11: p.Val559Gly
KIT 33	KIT mutant	*KIT* exon 11: p.Trp557Gly
KIT 34	KIT mutant	*KIT* exon 11: p.Val560Asp
KIT 35	KIT mutant	*KIT* exon 11: p.Val559Ala
KIT 37	KIT mutant	*KIT exon 11*: p.Trp557_Val559delinsPhe
KIT 38	KIT mutant	*KIT* exon 11 indel
KIT 39	KIT mutant	*KIT* exon 11: p.Trp557_Val559delinsCys
KIT 40	KIT mutant	*KIT* exon 11: p.Pro573_Glu583dup
PDGFRA 01	PDGFRA mutant	*PDGFRA* exon 14: p.Asn659Tyr; exon 18: p.Tyr849Cys
PDGFRA 02	PDGFRA mutant	*PDGFRA* exon 18: p.Asp842Val
PDGFRA 07	PDGFRA mutant	*PDGFRA* exon 18: p.Asp842Val
PDGFRA 14	PDGFRA mutant	*PDGFRA* exon 18: p.Asp842Ile
PDGFRA 15	PDGFRA mutant	*PDGFRA* exon 12: p.Val561Asp
PDGFRA 17	PDGFRA mutant	*PDGFRA* exon 18: p.Asp842Val
PDGFRA 19	PDGFRA mutant	*PDGFRA* exon 18: p.Asn842Lys
PDGFRA 23	PDGFRA mutant	*PDGFRA* exon 12: p.Val561Asp
PDGFRA 32	PDGFRA mutant	*PDGFRA* exon 18: p.Asp842Val
PDGFRA 36	PDGFRA mutant	*PDGFRA* exon 18: p.Asp842Val
WT 03	KIT/PDGFRA wild type	*SDHC* exon 4:p.Gly75Asp
WT 04	KIT/PDGFRA wild type	none identified
WT 05	KIT/PDGFRA wild type	none identified
WT 06	KIT/PDGFRA wild type	none identified
WT 10	KIT/PDGFRA wild type	*SDHA* exon 14: p.Tyr629Phe; exon 15: p.Val657Ile
WT 12	KIT/PDGFRA wild type	*SDHA* exon 7:p.Thr273Ile; exon 10:p.Gly453Arg
WT 18	KIT/PDGFRA wild type	none identified
WT 16[c]	KIT/PDGFRA wild type	none identified

[a]See Figure x
[b]Amino acid numbering from isoforms NP_000213.1 (KIT), NP_006197.1 (PDGFRA), NP_004159.2 (SDHA), NP_002992.1 (SDHC)
[c]SDH-intact WT

24
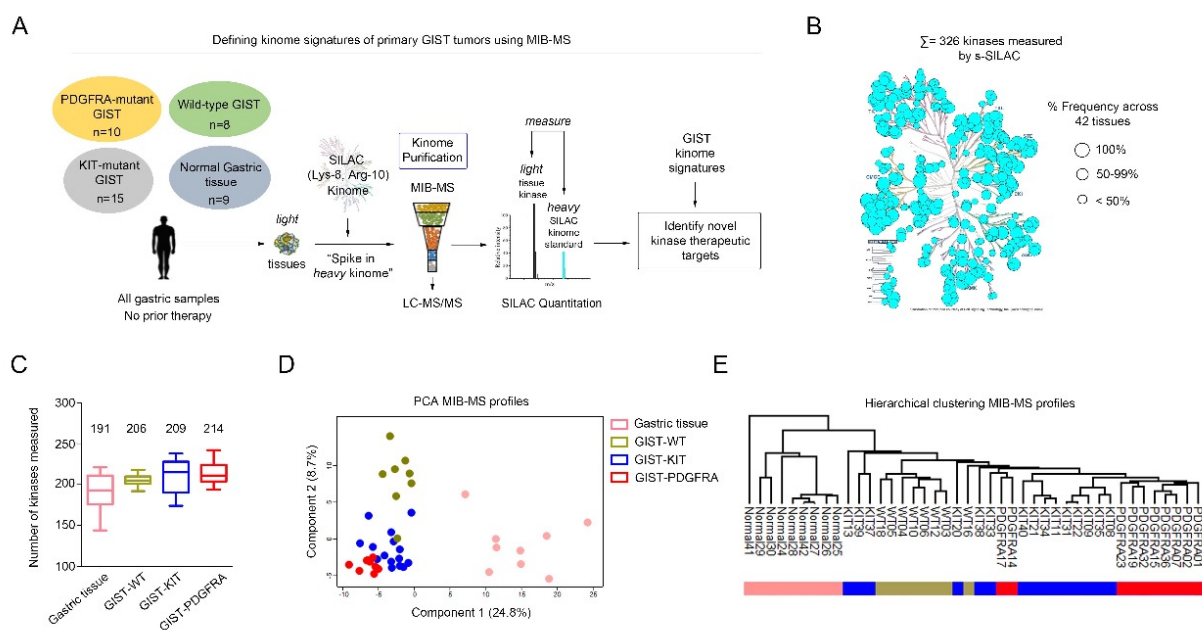
Figure 1.

Figure 1. Characterizing the GIST kinome in primary tumors using MIB-MS to identify novel therapeutic targets. **(A)** Schematic of experimental approach. An equal amount of SILAC-based kinome standard is added to each non-labeled sample (untreated, gastric primary GIST from three molecular subtypes: *KIT*-mutant, n=15; *PDGFRA*-mutant, n=10; wild-type GIST, n=8, and normal gastric tissue, n=9). MIB-MS was used to quantify the kinase abundance in GIST patient tumors to map the proteomic landscape of the kinome and identify novel targets. **(B)** Kinome tree depicts fraction of kinome quantitated by MIB-MS and frequency across 42 samples measured. **(C)** Number of kinases detected by MIB-MS profiling broken down by tissue type. **(D)** Principal Component Analysis of MIB-MS in three GIST subtypes (*KIT*-mutant (blue), *PDGFRA*-mutant (red), wild-type (green)) and normal gastric tissue (pink). **(E)** Hierarchical clustering of MIB-MS kinome profiles of 42 samples.

25
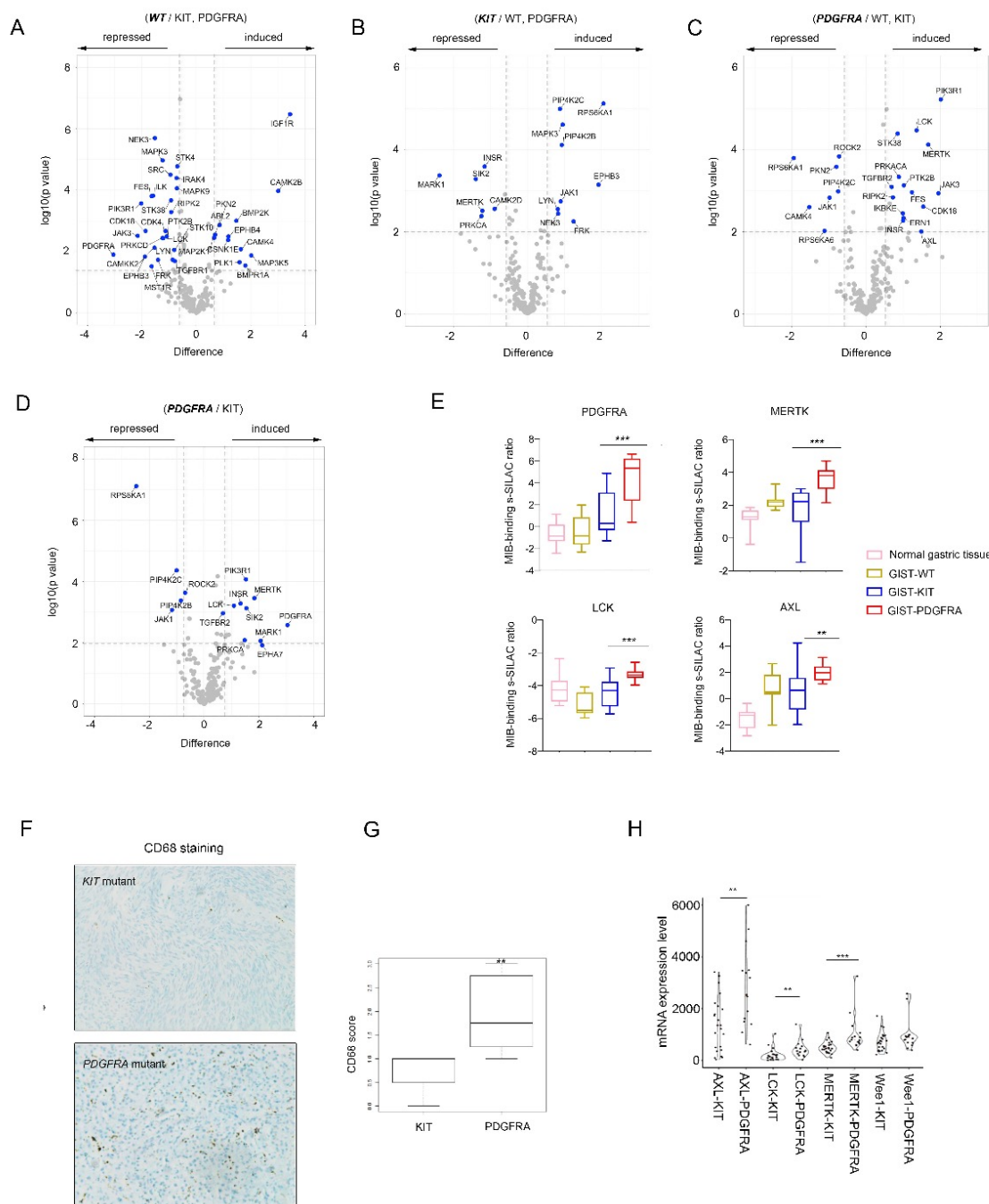
Figure 2

Figure 2. Mapping the distinct kinome signatures among GIST subtypes. **(A)** Volcano plot comparisons of wild-type, **(B)** *KIT*-mutant, **(C)** *PDGFRA*-mutant, and **(D)** *PDGFRA* versus *KIT*-

mutant GIST MIB-MS kinome profiles. Statistical differences in kinase $\log_2$ s-SILAC ratios comparing one GIST subtype versus other two subtypes were determined by paired *t* test Benjamini-Hochberg adjusted *P* valus at an FDR of <0.05. **(D)** Box plots show kinase abundance determined by Q-MIBs of *PDGFRA*-mutant subtype specific kinases, PDGFRA, MERTK, LCK and AXL. **(E)** Immunohisochemical analysis (IHC) of CD68 in representative untreated *KIT* (**top**) and *PDGFRA* (**bottom**) -mutant GIST. **(F)** Box-and-whisker plots of CD68 IHC scores in untreated *KIT* exon 11 (n=8) and *PDGFRA* D842V(n=8) -mutant GIST, p= 0.004, using two-sided Mann-Whitney test. **(G)** mRNA expression of AXL, LCK, MERTK and Wee1 in *KIT*-and *PDGFRA*-mutant primary GIST mined from an independent RNA-seq study (36). Violin plot shows all data points (black dots) and mean expression (red dots). p = <0.05; *KIT*-mutant, n= 23; *PDGFRA*-mutant, n= 16.
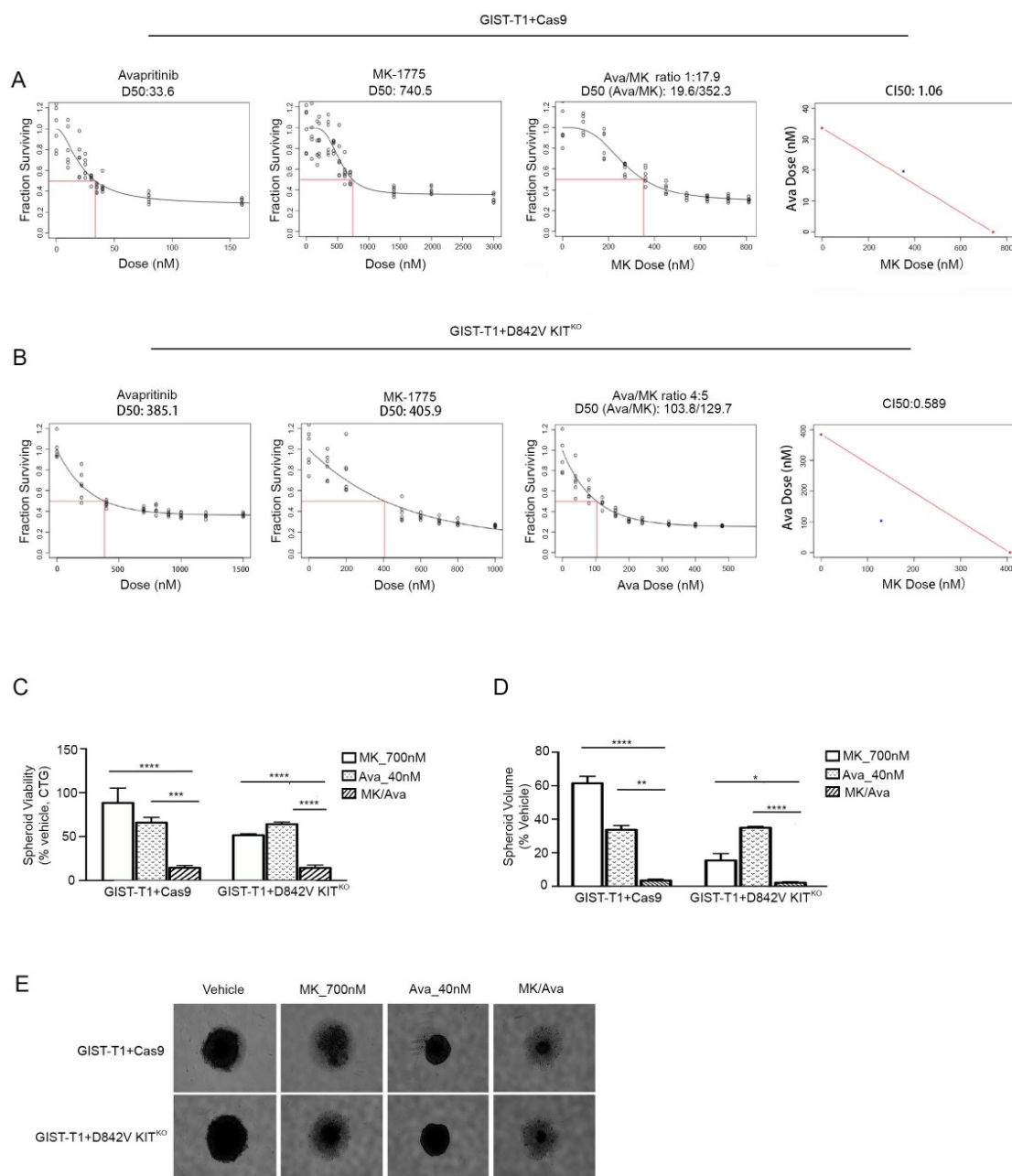
Figure 3
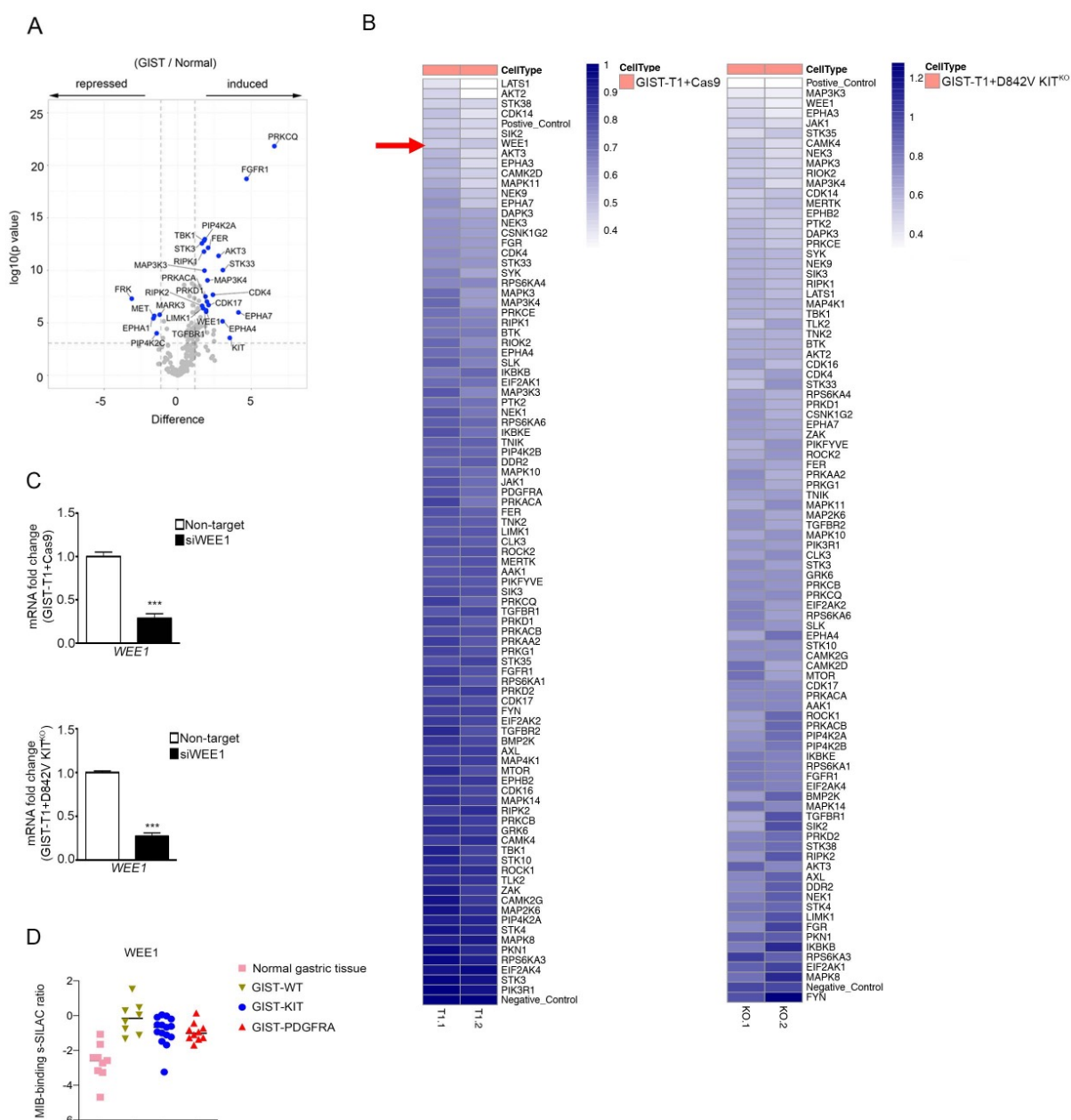
Figure 3. Targeting the GIST tumor kinome signature identifies WEE1 as candidate target

(A) Volcano plot comparisons of all GIST primary tumors and normal gastric tissue MIB-MS

kinome profiles. Statistical differences in kinase log$_2$ s-SILAC ratios comparing all GIST tumors

versus normal gastric tissue were determined by paired t test Benjamini-Hochberg adjusted P values at an FDR of <0.05. **(B)** Heatmap depicting viability scores for kinase-centric siRNA library screen in GIST-T1+Cas9 (**left**) and GIST-T1+D842V KIT^{KO} (**right**) cell lines as measured by Cell Titer Blue assay. siGL2 was negative control, viability score =1.0. Knockdown of Wee1 induced significant cytotoxicity in both cell lines (viability score = 0.48 in GIST-T1+Cas9; 0.41 in GIST-T1+D842V KIT^{KO}). Two independent replicates were performed in each cell line. **(C)** Quantitative RT-PCR confirmed >70% knockdown of Wee1 mRNA in both cell lines. Expression levels were normalized to HPRT. *** P < 0.0001. **(D)** Dot plots of Wee1 abundance in all 42 samples determined by Q-MIBs.
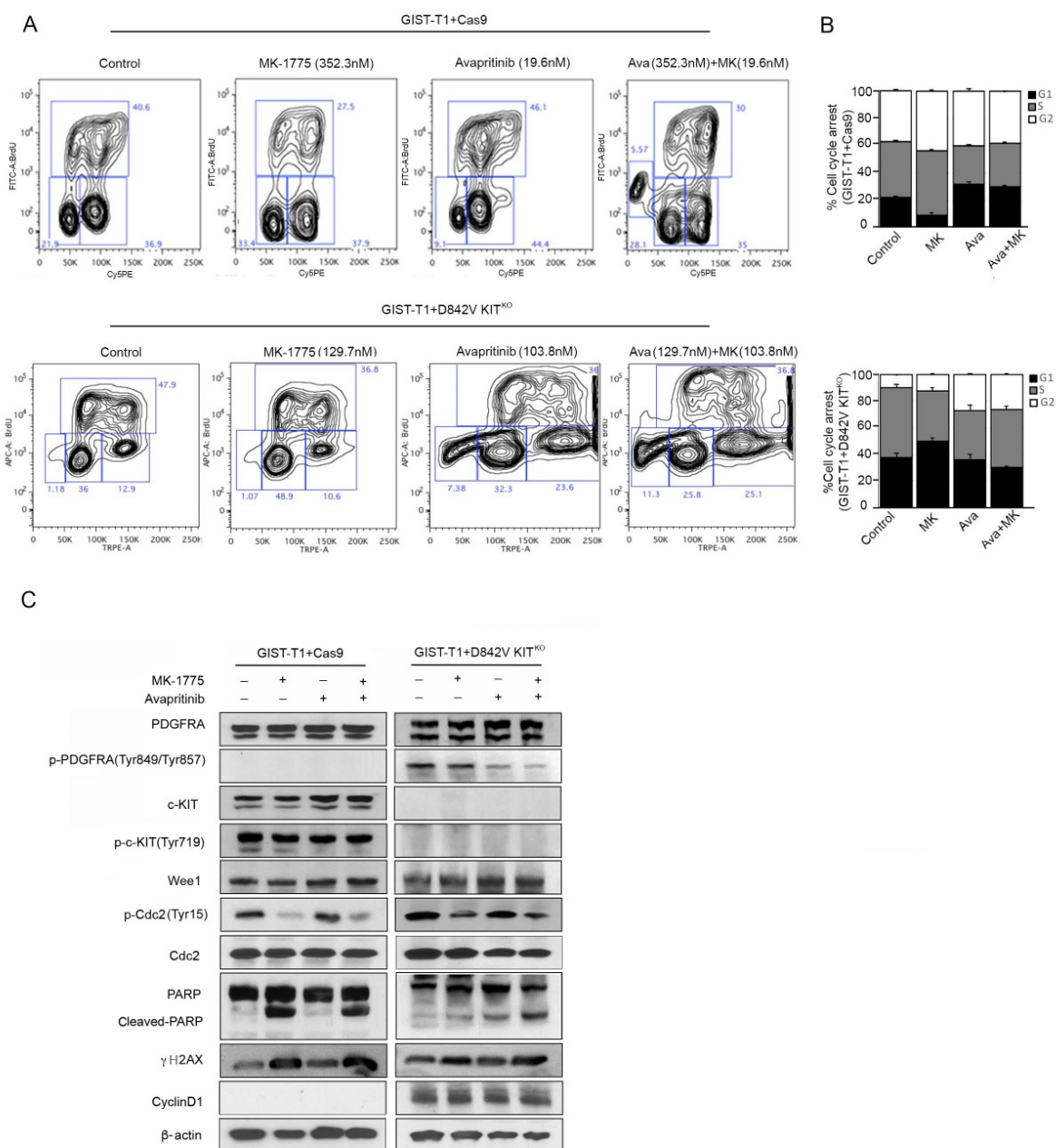
Figure 4

Figure 4. MK-1775 and avapritinib have enhanced combination on *in vitro* GIST cell growth

(A) Panels 1 & 2, Dose response curves for single agents (avapritinib, MK-1775) in GIST-T1+Cas9 cell line. Red box indicates estimation of LD50 concentration for each single drug. **Panel**

3, Dose response curve representing increasing series of combinations. Red box indicates estimation of LD50 concentration for combination of drugs. **Panel 4,** Single point (blue) on isobole curve for 50% kill. Red line indicates 50% isobole for strictly additive effect. CI_{LD50} is 1.06 and not found in the synergistic triangle (region below the red line). **(B) Panels 1 & 2**, Dose response curves for single agents (avapritinib, MK-1775) in GIST-T1+D842V KIT^{KO} cell line. Red box indicates estimation of LD50 concentration for each single drug. **Panel 3**, Dose response curve representing increasing series of combinations. Red box indicates estimation of LD50 concentration for combination of drugs. **Panel 4**, Single point on isobole curve (blue) for 50% kill. Red line indicates 50% isobole for strictly additive effect. CI_{LD50} is 0.589 and is found within the synergistic triangle. **(C)** Bars represent average viability $\pm$ SEM after 120-hour treatment at the indicated concentrations of drugs for GIST-T1+Cas9 and GIST-T1+D842V KIT^{KO} spheroids as a percentage of vehicle-treated spheroids. Viability was measured using the Cell Titer-Glo cell viability assay. **(D)** Spheroids were imaged after 120-hour treatments and surface area was calculated using ImageJ software. Surface area was converted to spheroid volume (50). Bars represent the average spheroid volume $\pm$ SEM of GIST-T1+Cas9 and GIST-T1+D842V KIT^{KO} spheroids as a percentage of vehicle-treated spheroids. All spheroid data were analyzed using GraphPad Prism, with comparisons of treatment groups performed in one-way ANOVA and post hoc comparisons made using Bonferroni multiple comparisons method * p = 0.0165, ** p =0.0046, *** p = 0.0008, **** p =< 0.0001. **(E)** Representative images of GIST-T1+Cas9 and GIST-T1+D842V KIT^{KO} spheroids after 120-hour treatment at the indicated concentrations.

31

Figure 5. Mechanism of MK-1775 and avapritinib combination in KIT-dependent and – independent GIST cell lines. **(A)** Representative flow cytometry plots and **(B)** quantification of BrdU incorporation in GIST-T1+Cas9 (**upper panel**) treated with 352.3nM MK-1775, 19.6nM

32

Avapritinib and combination for 72h. Statistically significant differences were observed between the following comparisons: for G1 arrest，vehicle vs. avapritinib ($p < 0.0009$) and vehicle vs. avapritinib/MK-1775 ($p < 0.0002$); for G2 arrest, vehicle vs. MK-1775 ($p < 0.005$). **(A)** Representative flow cytometry plots and **(B)** quantification of BrdU incorporation in GIST-T1-D842V+ KIT^{KO} treated **(bottom panel)** with 129.7nM MK-1775, 103.8nM Avaritinib and combination for 72h. Statistically significant differences were observed between the following comparisons: for G1 arrest，vehicle vs. MK-1775 ($p < 0.0001$); for G2 arrest, vehicle vs. avapritinib ($p < 0.005$), vehicle vs. avapritinib/MK-1775 ($p < 0.0002$). **(C)** Immunoblot assays of WCEs from GIST-T1+Cas9 (KIT-dependent) and GIST-T1+D842V KIT^{KO} (KIT-independent) cell lines treated as in (**A, B**). Equal concentrations (45-90ug) of WCE from each sample were subjected to immunoblotting with specific antibodies, as indicated. β-actin served as a loading control.

Figure 6
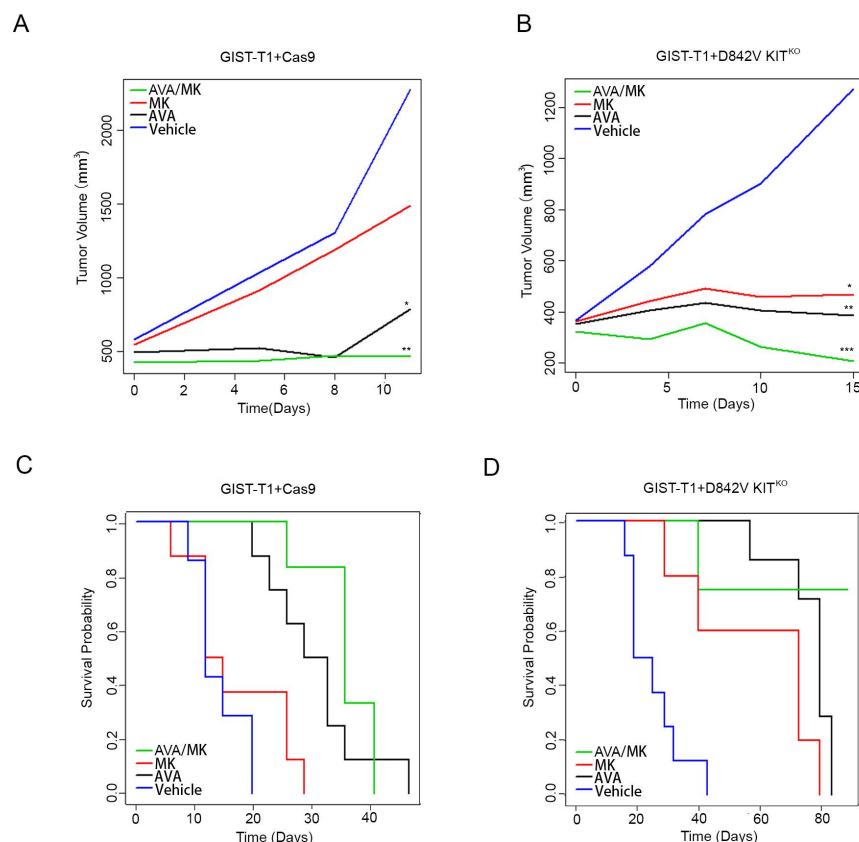
Figure 6. The combination of MK-1775 and avapritinib significantly inhibits GIST growth *in vivo* and improves disease-specific survival. **(A)** Statistically significant decreases in the rate of GIST-T1+Cas9 xenograft tumor growth were observed due to treatment with avapritinib（* p = 0.05 , black) and avapritinib+MK-1775 combination (** p = 0.002, green) compared with vehicle group (blue) at day 11. **(B)** Statistically significant decreases in the rate of GIST-T1+D842V KIT^{KO} xenograft tumor growth were observed due to treatment with avapritinib (** p = 0.002) and MK-1775 (* p = 0.02) and avapritinib+MK-1775 (*** p = < 0.0002) compared to vehicle group at day 15. Smoothed tumor growth curves (tumor volume vs. time) were computed for each treatment

using the lowess smoother in the R statistical language. **(C)** Kaplan-Meier estimate of the probability of disease-specific survival of GIST-T1+Cas9 xenografts. Statistically significant differences (even after adjusting for multiple testing) in disease-specific survival were observed between the following comparisons: Vehicle vs. avapritinib ($p < 0.0001$), vehicle vs. avapritinib/MK-1775 ($p < 0.0001$), and MK-1775 vs. avapritinib/MK-1775 ($p < 0.0001$). **D)** Kaplan-Meier estimate of the probability of disease-specific survival of GIST-T1+D842V KIT^{KO} xenografts. Statistically significant differences (even after adjusting for multiple testing) in disease-specific survival were observed between the following comparisons: Vehicle vs. MK-1775 ($p = 0.01$), vehicle vs. avapritinib ($p < 0.0001$), vehicle vs. avapritinib/MK-1775 ($p<0.0001$), MK-1775 vs. avapritinib/MK-1775 ($p = 0.01$) and avapritinib vs. avapritinib/MK-1775 ($p = 0.02$) are significant. The overall test is also significant ($p < 0.0001$).

Literature Cited

1. Goettsch WG, Bos SD, Breekveldt-Postma N, Casparie M, Herings RM, Hogendoorn PC: **Incidence of gastrointestinal stromal tumours is underestimated: results of a nation-wide study**. *Eur J Cancer* 2005, **41**(18):2868-2872.
2. Heinrich MC, Corless CL, Duensing A, McGreevey L, Chen CJ, Joseph N *et al*: **PDGFRA activating mutations in gastrointestinal stromal tumors**. *Science* 2003, **299**(5607):708-710.
3. Belinsky MG, Rink L, Flieder DB, Jahromi MS, Schiffman JD, Godwin AK *et al*: **Overexpression of insulin-like growth factor 1 receptor and frequent mutational inactivation of SDHA in wild-type SDHB-negative gastrointestinal stromal tumors**. *Genes, chromosomes & cancer* 2013, **52**(2):214-224.
4. Killian JK, Miettinen M, Walker RL, Wang Y, Zhu YJ, Waterfall JJ *et al*: **Recurrent epimutation of SDHC in gastrointestinal stromal tumors**. *Sci Transl Med* 2014, **6**(268):268ra177.
5. Debiec-Rychter M, Sciot R, Le Cesne A, Schlemmer M, Hohenberger P, van Oosterom AT *et al*: **KIT mutations and dose selection for imatinib in patients with advanced gastrointestinal stromal tumours**. *European journal of cancer* 2006, **42**(8):1093-1103.

6. Wozniak A, Rutkowski P, Schoffski P, Ray-Coquard I, Hostein I, Schildhaus HU *et al*: **Tumor genotype is an independent prognostic factor in primary gastrointestinal stromal tumors of gastric origin: a european multicenter analysis based on ConticaGIST**. *Clin Cancer Res* 2014, **20**(23):6105-6116.

7. Rossi S, Gasparotto D, Miceli R, Toffolatti L, Gallina G, Scaramel E *et al*: **KIT, PDGFRA, and BRAF Mutational Spectrum Impacts on the Natural History of Imatinib-naive Localized GIST: A Population-based Study**. *The American journal of surgical pathology* 2015.

8. Cassier PA, Fumagalli E, Rutkowski P, Schoffski P, Van Glabbeke M, Debiec-Rychter M *et al*: **Outcome of patients with platelet-derived growth factor receptor alpha-mutated gastrointestinal stromal tumors in the tyrosine kinase inhibitor era**. *Clinical cancer research : an official journal of the American Association for Cancer Research* 2012, **18**(16):4458-4464.

9. Heinrich MC, Owzar K, Corless CL, Hollis D, Borden EC, Fletcher CD *et al*: **Correlation of kinase genotype and clinical outcome in the North American Intergroup Phase III Trial of imatinib mesylate for treatment of advanced gastrointestinal stromal tumor: CALGB 150105 Study by Cancer and Leukemia Group B and Southwest Oncology Group**. *J Clin Oncol* 2008, **26**(33):5360-5367.

10. Evans EK, Gardino AK, Kim JL, Hodous BL, Shutes A, Davis A *et al*: **A precision therapy against cancers driven by KIT/PDGFRA mutations**. *Sci Transl Med* 2017, **9**(414).

11. Gebreyohannes YK, Wozniak A, Zhai ME, Wellens J, Cornillie J, Vanleeuw U *et al*: **Robust Activity of Avapritinib, Potent and Highly Selective Inhibitor of Mutated KIT, in Patient-derived Xenograft Models of Gastrointestinal Stromal Tumors**. *Clin Cancer Res* 2019, **25**(2):609-618.

12. Heinrich MC JR, von Mehren M, Schoffski P, Serrano C, Kang YK, Cassier P, Mir O, Eskens F, Tap WD, Rutkowski P, Chawla SP, Trent J, Tugnait M, Evans EK, Lauz T, Zhou T, Roche M, Wolf BB, Bauer S and George S.: **Avapritinib in advanced PDGFRA D842V-mutant gastrointestinal stromal tumor (NAVIGATOR): a multicenter, open-label, phase 1 trial**. *Lancet Oncology* 2020.

13. Subramanian S, West RB, Corless CL, Ou W, Rubin BP, Chu KM *et al*: **Gastrointestinal stromal tumors (GISTs) with KIT and PDGFRA mutations have distinct gene expression profiles**. *Oncogene* 2004, **23**(47):7780-7790.

14. Indio V, Astolfi A, Tarantino G, Urbini M, Patterson J, Nannini M *et al*: **Integrated Molecular Characterization of Gastrointestinal Stromal Tumors (GIST) Harboring the Rare D842V Mutation in PDGFRA Gene**. *Int J Mol Sci* 2018, **19**(3).

15. Roskoski R, Jr.: **Properties of FDA-approved small molecule protein kinase inhibitors**. *Pharmacol Res* 2019, **144**:19-50.

16. Knapp S, Arruda P, Blagg J, Burley S, Drewry DH, Edwards A *et al*: **A public-private partnership to unlock the untargeted kinome**. *Nat Chem Biol* 2013, **9**(1):3-6.

17. Bantscheff M, Eberhard D, Abraham Y, Bastuck S, Boesche M, Hobson S *et al*: **Quantitative chemical proteomics reveals mechanisms of action of clinical ABL kinase inhibitors**. *Nat Biotechnol* 2007, **25**(9):1035-1044.

18. Duncan JS, Whittle MC, Nakamura K, Abell AN, Midland AA, Zawistowski JS *et al*: **Dynamic reprogramming of the kinome in response to targeted MEK inhibition in triple-negative breast cancer**. *Cell* 2012, **149**(2):307-321.

19.   Franks CE, Hsu KL: **Activity-Based Kinome Profiling Using Chemical Proteomics and ATP Acyl Phosphates**. *Curr Protoc Chem Biol* 2019, **11**(3):e72.

20.   Kurimchak AM, Herrera-Montavez C, Brown J, Johnson KJ, Sodi V, Srivastava N *et al*: **Functional proteomics interrogation of the kinome identifies MRCKA as a therapeutic target in high-grade serous ovarian carcinoma**. *Sci Signal* 2020, **13**(619).

21.   Johnson KJ, Kumar V, Kurimchak AM, Srivastava N, Peri S, Cai KQ *et al*: **Kinome Profiling of Primary Endometrial Tumors Using Multiplexed Inhibitor Beads and Mass Spectrometry Identifies SRPK1 As Candidate Therapeutic Target**. *bioRxiv* 2020:2020.2003.2003.970251.

22.   Deeb SJ, D'Souza RC, Cox J, Schmidt-Supprian M, Mann M: **Super-SILAC allows classification of diffuse large B-cell lymphoma subtypes by their protein expression profiles**. *Mol Cell Proteomics* 2012, **11**(5):77-89.

23.   Belinsky MG, Cai KQ, Zhou Y, Luo B, Pei J, Rink L *et al*: **Succinate dehydrogenase deficiency in a PDGFRA mutated GIST**. *BMC Cancer* 2017, **17**(1):512.

24.   Taguchi T, Sonobe H, Toyonaga S, Yamasaki I, Shuin T, Takano A *et al*: **Conventional and molecular cytogenetic characterization of a new human cell line, GIST-T1, established from gastrointestinal stromal tumor**. *Lab Invest* 2002, **82**(5):663-665.

25.   Greco WR, Bravo G, Parsons JC: **The search for synergy: a critical review from a response surface perspective**. *Pharmacol Rev* 1995, **47**(2):331-385.

26.   Zook P, Pathak HB, Belinsky MG, Gersz L, Devarajan K, Zhou Y *et al*: **Combination of Imatinib Mesylate and AKT Inhibitor Provides Synergistic Effects in Preclinical Study of Gastrointestinal Stromal Tumor**. *Clin Cancer Res* 2017, **23**(1):171-180.

27.   Tarn C, Skorobogatko YV, Taguchi T, Eisenberg B, von Mehren M, Godwin AK: **Therapeutic effect of imatinib in gastrointestinal stromal tumors: AKT signaling dependent and independent mechanisms**. *Cancer Res* 2006, **66**(10):5477-5486.

28.   Gill AJ, Chou A, Vilain R, Clarkson A, Lui M, Jin R *et al*: **Immunohistochemistry for SDHB divides gastrointestinal stromal tumors (GISTs) into 2 distinct types**. *Am J Surg Pathol* 2010, **34**(5):636-644.

29.   Oppermann FS, Gnad F, Olsen JV, Hornberger R, Greff Z, Keri G *et al*: **Large-scale proteomics analysis of the human kinome**. *Mol Cell Proteomics* 2009, **8**(7):1751-1764.

30.   Tarn C, Rink L, Merkel E, Flieder D, Pathak H, Koumbi D *et al*: **Insulin-like growth factor 1 receptor is a potential therapeutic target for gastrointestinal stromal tumors**. *Proc Natl Acad Sci U S A* 2008, **105**(24):8387-8392.

31.   Rink L, Godwin AK: **Clinical and molecular characteristics of gastrointestinal stromal tumors in the pediatric and young adult population**. *Curr Oncol Rep* 2009, **11**(4):314-321.

32.   Rotert JV, Leupold J, Hohenberger P, Nowak K, Allgayer H: **Src activity is increased in gastrointestinal stromal tumors--analysis of associations with clinical and other molecular tumor characteristics**. *J Surg Oncol* 2014, **109**(6):597-605.

33.   Rossi F, Yozgat Y, de Stanchina E, Veach D, Clarkson B, Manova K *et al*: **Imatinib upregulates compensatory integrin signaling in a mouse model of gastrointestinal stromal tumor and is more effective when combined with dasatinib**. *Mol Cancer Res* 2010, **8**(9):1271-1283.

34.   Romeo S, Debiec-Rychter M, Van Glabbeke M, Van Paassen H, Comite P, Van Eijk R *et al*: **Cell Cycle/Apoptosis Molecule Expression Correlates with Imatinib Response in**

Patients with Advanced Gastrointestinal Stromal Tumors. *Clinical Cancer Research* 2009, **15**(12):4191-4198.

35. Duensing A, Medeiros F, McConarty B, Joseph NE, Panigrahy D, Singer S *et al*: **Mechanisms of oncogenic KIT signal transduction in primary gastrointestinal stromal tumors (GISTs)**. *Oncogene* 2004, **23**(22):3999-4006.

36. Vitiello GA, Bowler TG, Liu M, Medina BD, Zhang JQ, Param NJ *et al*: **Differential immune profiles distinguish the mutational subtypes of gastrointestinal stromal tumor**. *J Clin Invest* 2019, **129**(5):1863-1877.

37. Duensing A, Joseph NE, Medeiros F, Smith F, Hornick JL, Heinrich MC *et al*: **Protein Kinase C theta (PKCtheta) expression and constitutive activation in gastrointestinal stromal tumors (GISTs)**. *Cancer Res* 2004, **64**(15):5127-5131.

38. Li F, Huynh H, Li X, Ruddy DA, Wang Y, Ong R *et al*: **FGFR-Mediated Reactivation of MAPK Signaling Attenuates Antitumor Effects of Imatinib in Gastrointestinal Stromal Tumors**. *Cancer Discov* 2015, **5**(4):438-451.

39. Ou WB, Ni N, Zuo R, Zhuang W, Zhu M, Kyriazoglou A *et al*: **Cyclin D1 is a mediator of gastrointestinal stromal tumor KIT-independence**. *Oncogene* 2019, **38**(39):6615-6629.

40. Pantaleo MA, Nannini M, Corless CL, Heinrich MC: **Quadruple wild-type (WT) GIST: defining the subset of GIST that lacks abnormalities of KIT, PDGFRA, SDH, or RAS signaling pathways**. *Cancer Med* 2015, **4**(1):101-103.

41. Pantaleo MA, Tarantino G, Agostinelli C, Urbini M, Nannini M, Saponara M *et al*: **Immune microenvironment profiling of gastrointestinal stromal tumors (GIST) shows gene expression patterns associated to immune checkpoint inhibitors response**. *Oncoimmunology* 2019, **8**(9):e1617588.

42. Balachandran VP, Cavnar MJ, Zeng S, Bamboat ZM, Ocuin LM, Obaid H *et al*: **Imatinib potentiates antitumor T cell responses in gastrointestinal stromal tumor through the inhibition of Ido**. *Nat Med* 2011, **17**(9):1094-1100.

43. Seifert AM, Zeng S, Zhang JQ, Kim TS, Cohen NA, Beckman MJ *et al*: **PD-1/PD-L1 Blockade Enhances T-cell Activity and Antitumor Efficacy of Imatinib in Gastrointestinal Stromal Tumors**. *Clin Cancer Res* 2017, **23**(2):454-465.

44. Zhang JQ, Zeng S, Vitiello GA, Seifert AM, Medina BD, Beckman MJ *et al*: **Macrophages and CD8(+) T Cells Mediate the Antitumor Efficacy of Combined CD40 Ligation and Imatinib Therapy in Gastrointestinal Stromal Tumors**. *Cancer Immunol Res* 2018, **6**(4):434-447.

45. Matheson CJ, Backos DS, Reigan P: **Targeting WEE1 Kinase in Cancer**. *Trends Pharmacol Sci* 2016, **37**(10):872-881.

46. Yang L, Shen C, Pettit CJ, Li T, Hu AJ, Miller ED *et al*: **Wee1 Kinase Inhibitor AZD1775 Effectively Sensitizes Esophageal Cancer to Radiotherapy**. *Clin Cancer Res* 2020.

47. Kong A, Good J, Kirkham A, Savage J, Mant R, Llewellyn L *et al*: **Phase I trial of WEE1 inhibition with chemotherapy and radiotherapy as adjuvant treatment, and a window of opportunity trial with cisplatin in patients with head and neck cancer: the WISTERIA trial protocol**. *BMJ Open* 2020, **10**(3):e033009.

48. Deneka AY, Einarson MB, Bennett J, Nikonova AS, Elmekawy M, Zhou Y *et al*: **Synthetic Lethal Targeting of Mitotic Checkpoints in HPV-Negative Head and Neck Cancer**. *Cancers (Basel)* 2020, **12**(2).

49.   Liu W, Zeng X, Yin Y, Li C, Yang W, Wan W *et al*: **Targeting the WEE1 kinase strengthens the antitumor activity of imatinib via promoting KIT autophagic degradation in gastrointestinal stromal tumors**. *Gastric Cancer* 2020, **23**(1):39-51.

50.   Ivanov DP, Parker TL, Walker DA, Alexander C, Ashford MB, Gellert PR *et al*: **Multiplexing spheroid volume, resazurin and acid phosphatase viability assays for high-throughput screening of tumour spheroids and stem cell neurospheres**. *PLoS One* 2014, **9**(8):e103817.